One-Dimensional Productivity Assessment for On-Field Methane Hydrate Production Using CO_2/N_2 Mixture Gas

Dong-Yeun Koh, Yun-Ho Ahn, Hyery Kang, and Seongmin Park
Dept. of Chemical and Biomolecular Enginieering, Korea Advanced Institute of Science and Technology, 373-1 Yuseong-gu, Daejeon 305–701, South Korea

Joo Yong Lee, Se-Joon Kim, and Jaehyoung Lee
Petroleum and Marine Research Div., Korea Institute of Geoscience and Mineral Resources, Gwahang-no 92, 30, Yuseong-gu, Daejeon 305–350, South Korea

Huen Lee
Dept. of Chemical and Biomolecular Enginieering, Korea Advanced Institute of Science and Technology, 373-1 Yuseong-gu, Daejeon 305–701, South Korea

Graduate School of EEWS, Korea Advanced Institute of Science and Technology, 373-1 Guseong-dong, Yuseong-gu, Daejeon 305–701, South Korea

DOI 10.1002/aic.14687
Published online November 29, 2014 in Wiley Online Library (wileyonlinelibrary.com)

The direct recovery of methane from gas hydrate-bearing sediments is demonstrated, where a gaseous mixture of $CO_2 + N_2$ is used to trigger a replacement reaction in complex phase surroundings. A one-dimensional high-pressure reactor (8 m) was designed to test the actual aspects of the replacement reaction occurring in natural gas hydrate (NGH) reservoir conditions. NGH can be converted into CO_2 hydrate by a "replacement mechanism," which serves double duty as a means of both sustainable energy source extraction and greenhouse gas sequestration. The replacement efficiency controlling totally recovered CH_4 amount is inversely proportional to $CO_2 + N_2$ injection rate which directly affecting solid - gas contact time. Qualitative/quantitative analysis on compositional profiles at each port reveals that the length more than 5.6 m is required to show noticeable recovery rate for NGH production. These outcomes are expected to establish the optimized key process variables for near future field production tests. © 2014 American Institute of Chemical Engineers *AIChE J*, 61: 1004–1014, 2015
Keywords: energy, gas hydrate, methane, carbon dioxide, replacement

Introduction

Natural gas hydrate (NGH), one of the most famous unconventional energy resources,[1] has recently opened its promising next stage as a double-duty source for natural gas production, and carbon dioxide sequestration. In 2012/2013, two gas hydrate field production tests were completed on/offshore: (1) The onshore field test was performed in 2012 on the Alaska North Slope in US to investigate the potential for CH_4—CO_2 replacement as a methane hydrate production method;[2] (2) The first offshore gas hydrate field test was attempted in 2013 on the Eastern Nankai Trough in Japan, where a depressurization technique was adopted for producing methane.[3] Most sites where NGH occurs have low accessibility and harsh engineering conditions; therefore, they are treated as difficult engineering energy resources. However, these recent attempts suggest that engineering barriers are now decreasing, and the next level approach is needed for NGH production R&D to examine the exact behavior of gas hydrates under realistic production conditions. Estimated technically recoverable gas hydrates in global volumes is in the order of approximately 3×10^{13} m^3, which is an amount similar to the shale-gas (~665Tcf) deposited in United States.[1,4] If the NGH produced on-site could gain price competitiveness against shale-gas, which is currently around \$3–4 MMBtu, NGH can take one big volume in the future global gas consumption. Accordingly, in Korea, two Ulleung Basin Gas Hydrate (UBGH) drilling expeditions were performed, in 2007 and 2010, revealing significant gas hydrate saturations in the sandy deposits, and the projects evaluated potential sites of future production tests.[5] An offshore gas hydrate field production test is scheduled for mid-2015 at the Ulleung Basin located in the East Sea of the Korean Peninsula.

One of the most attractive potential uses of gas hydrate is that it might serve as geologic reservoir for CO_2 sequestration in the deep sea floor.[6] The concept of (CH_4)—$(CO_2 + N_2)$ replacement (i.e., swapping or exchange) for methane production during sequestration of carbon dioxide gas in hydrate-bearing sediment is a plausible and potential approach that

Additional Supporting Information may be found in the online version of this article.

Correspondence concerning this article should be addressed to H. Lee at hlee@kaist.ac.kr or J. Lee at ljh1155@kigam.re.kr.

differs considerably from thermally stimulated and mechanically depressurized technologies.[7–10] Such a gas exchange inside the hydrate lattices has critical advantages over conventional NGH production methods. First, it is a nondestructive process of replacing CH_4 molecules in the hydrate cage with CO_2 molecules, thus, providing a dual mechanism of energy production and greenhouse gas sequestration.[7,11–19] Second, the direct use of the $CO_2 + N_2$ gas mixture (typically 20 mol % of CO_2 and 80 mol % of N_2 to reproduce the flue gas from a power plant) instead of pure CO_2 can greatly improve the overall CH_4 recovery rate and reduce additional CO_2 separation cost.[8] Engineering problems triggered by pure CO_2 injection, such as, CO_2 liquefaction during injection into the hydrate reservoir and related pipeline clogging problems, would be readily controlled when using the $CO_2 + N_2$ gas mixture because it still remains as a gaseous phase under most deep sea conditions. Third, serious concerns about massive amounts of water naturally coming from NGH dissociation can be greatly resolved. Here, we note again that the nondestructive replacement process preserves host water lattice (sI hydrate) in the gas hydrate-bearing sediment as part of the newly formed CO_2 (or $CO_2 + N_2$) hydrates. Conversely, all of the depressurization, thermal stimulation and inhibitor injection techniques require large volumes of water to be displaced from gas hydrate-bearing sediment. Furthermore, the ensuing endothermic temperature drop caused by depressurization can result in undesirable formation of secondary methane hydrate or ice in the well and near the well bore region.[20,21] The chemical exchange of dissimilar guest molecules does not produce significant cooling, but makes only negligible sensitive heat.[22] Fourth, the geomechanical stability of gas hydrate-bearing sediment is not threatened. Shallow gas hydrate-bearing sediments (Bottom Simulating Reflector depth < 200 m) are poorly consolidated (or unconsolidated) and the hydrate provides mechanical integrity as bonding material.[23]

The earlier microscopic experiments on CH_4—CO_2 exchange reported that the CH_4 recovery yield of CO_2 replacement was 64% while the $CO_2 + N_2$ gas mixture achieved 84% for sI gas hydrate.[8] The additional results were that, for sII and sH gas hydrate, the $(CO_2 + N_2)$—CH_4 replacement had more than a 90% CH_4 recovery rate followed by structural transition phenomenon from sII or sH to sI.[9] Recent microsecond molecular dynamics study revealed nondestructive mechanism of CH_4—CO_2 replacement process.[24] The use of $CO_2 + N_2$ mixed gas becomes practically acceptable to NGH production, because it not only reduces real process barriers but also increases CH_4 recovery yield. More recently, continued efforts have been made to simulate actual gas hydrate replacement reactions in lab-scale experiments. Zhou et al. compared the replacement kinetics at different concentrations of CO_2 in carbon dioxide-in-water emulsions and analyzed the proper replacement temperature and pressure conditions according to the thermodynamic phase equilibria.[25,26] Yuan et al. investigated the effect of water on the CH_4—CO_2 replacement reaction and proposed a kinetic model.[27] Furthermore, Yuan et al. evaluated the gas hydrate reservoir conditions for favorable liquid CO_2 injection conditions.[28] Hirohama et al. and Ota et al. measured the replacement rate and concluded that final reaction time have some deviations up to 20–300 h.[29–31] Such differences in reaction time can be mainly attributed to reaction conditions (temperature and pressure) and phases of the CH_4 hydrate (bulk or powder). Moreover, the CH_4 hydrate is known to have a self-preservation effect, so that when the guest exchange reaction occurs at sub-zero temperatures it can be inhibited by slower hydrate dissociation or slower mass transfer.[17] As Ota et al. reported, the guest exchange reaction showed better efficiency when liquid CO_2 was used instead of gaseous CO_2 (which is attributable to the increased contact area between liquid CO_2 and solid CH_4 hydrate), and to an experimental temperature above 0°C where the self-preservation effect is not observed.[29,30] However, it should be noted that the limiting value of the gas exchange is still around 64%, although the reaction rate is increased with increased contact area.[7] More recently, Lee et al.[32] performed the CO_2—CH_4 replacement experiments using liquid CO_2 and proposed the CO_2—CH_4 exchange mechanism based on soaking time and diffusive penetration depth in gas hydrate particles. The authors claimed that a longer soak time limited the diffusion of CO_2 through preformed gas hydrate layer and thus decreasing the exchange rate.

A complete understanding of the CO_2 replacement mechanism of NGH in a complex sediment structure composed of sands, silts, and clays is essential for the exploitation of deep-sea NGH deposits. The porosity is relatively high in sand but low in silt and clay. In previous studies, we preliminarily analyzed precise cage occupancy and phase behavior of NGH, revealing a significant methane population in the layered structure of natural sediments.[33,34] Naturally occurring gas hydrates are distributed in various types of geologic sediments. The pore-filling hydrate structure is confirmed from recent seismic survey studies in gas hydrate field of Blake Ridge,[35,36] Alaska,[36] and Mackenzie Delta[37] gas hydrate fields. Also in UBGH sites have sandy-sediment type and pore-filling structure of CH_4 hydrate was confirmed.[5] In UBGH sites, most NGH sediments are composed of alternate layers having two distinct parts of sand and clay layers (Figure 1a). Even though clay layers contain a considerable amount of gas hydrate in the form of intercalated methane hydrate, clay layers are considered to be practically impermeable due to compact packing between clay particles.[38] In contrast, sand layers also contain a significant amount of gas hydrates and they are considered to be practically permeable. Thus, we mainly focus on the sand layers in the gas hydrate reservoir as a technically recoverable hydrate.

In this research, we use a $CO_2 + N_2$ gas mixture for on/offshore NGH production, focusing on the following two issues: (1) mixed fluid flow characteristics of CH_4, CO_2, and N_2 in geologically sandy media. Due to the alternated layers of clay and sand, the target sand layer is considered as a conduit-like layer and needed to be simulated to investigate realistic fluid flow characteristics. We adopted continuous injection of $CO_2 + N_2$ gas mixture into methane hydrates. Continuous gas injection allowed us to observe different aspect of replacement behavior of gas hydrates such as replacement efficiency dependence on gas injection rate, confirmation of gas hydrate replacement reaction under continuous gas flow, and determination of minimum gas injection rate/length according to the replacement efficiency. (2) Replacement efficiency in relation to a one-dimensional (1-D) length scale. To minimize the other gas diffusion directions, we applied 1-D scale experiments and observed gas flow under strictly controlled environment. Ideal CH_4—$(CO_2 + N_2)$ replacement efficiency is reported 85%.[8] However, our experimental results suggest

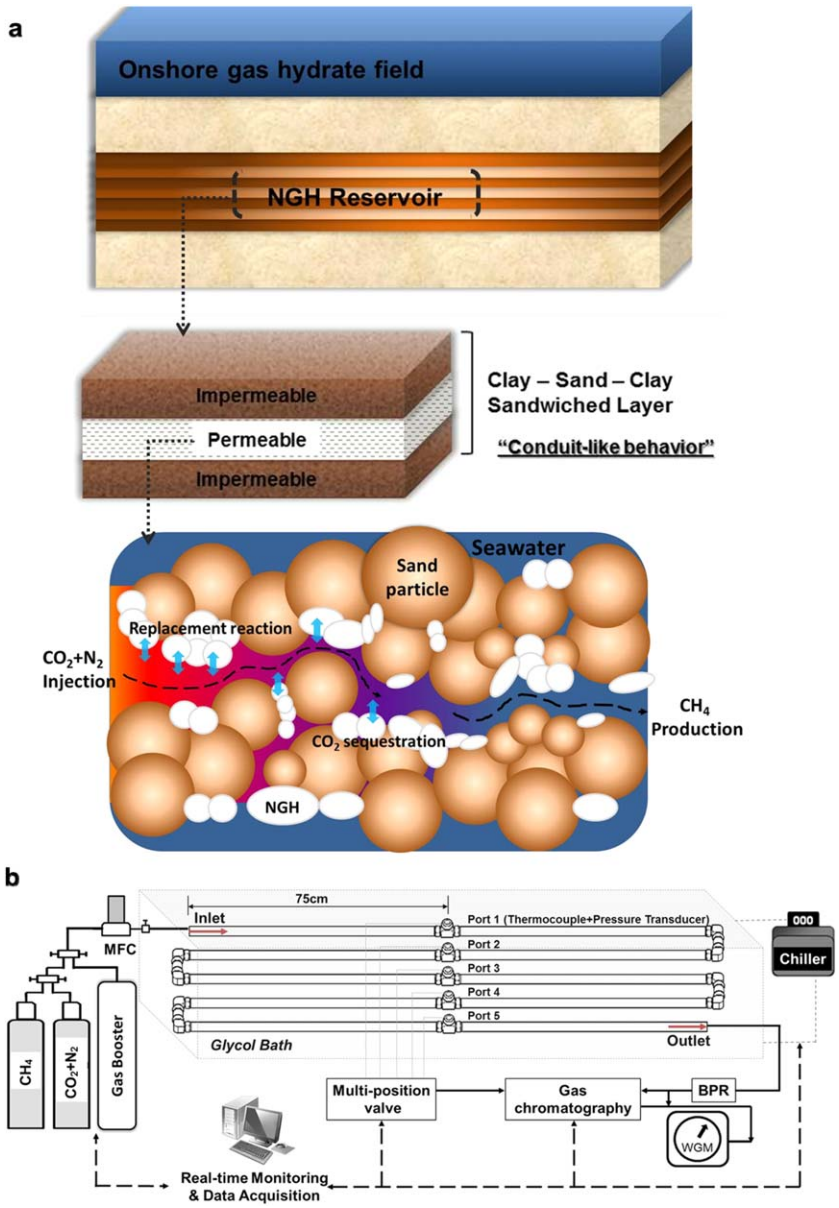

Figure 1. (a) Schematic illustration of CH_4—(CO_2 + N_2) replacement occurring in the NGH reservoir; (b) schematic diagram of experimental apparatus.

[Color figure can be viewed in the online issue, which is available at wileyonlinelibrary.com.]

that replacement efficiency could be lowered below 50% and significantly differed by gas injection length. The complete characterization of fluid flow occurring in the NGH sediments during CH_4—($CO_2 + N_2$) replacement make process variables of well design (injection/production), NGH reservoir length, produced CH_4 duration and total CH_4 recovery rate. For close simulation of actual alternate layers of deep-sea NGH, we designed a 8 m experimental setup and a 1-D tubular reactor (Figure 1b) and investigated the fluid flow characteristics and replacement mechanisms along the length as the preliminary first approach.

Experimental Section

One-dimensional 8 m high-pressure vessel

Figure 1b shows a schematic diagram of the apparatus and its components. A high-pressure vessel was constructed using 316 stainless steel tubes, which has pressure rating of 350 bar. The dimensions of the tube-type high-pressure vessel were 1.65 cm for the inner diameter (outer diameter = 1.905 cm) and 800 cm for the total length. The sampling ports for the inner fluid were installed at intervals of 160 cm at 0.7, 2.4, 4.0, 5.6, and 7.3 m. The gas samples taken at each port were transferred to a multiposition valve (EMTCSD10UW, Valco) and subsequently processed by gas chromatography (GC). At the sampling ports, the 4-wire PT-100 thermocouple probe and pressure transducer (UNIK 5000, GE) with a line filter were installed. The pressure vessel was placed in the glycol bath and an external chiller was used to precisely control the bath temperature during the experiments.

Fluid control and property measurement system

A dual-syringe pump (Teledyne Isco, 500D) was used to inject ultrapure water into the reactor. Mass flow controllers (Brooks, model 5850E) were used to control the injection

rates of CH_4 and $CO_2 + N_2$ mixture gas. A system control and monitoring program was developed, using the National Instrument LabVIEW, for the data acquisition and user-friendly control of the apparatus while the entire experiment was observed in real time. A wet gas meter (W-NK-1, Shinagawa) was used to measure the produced gas volume. GC (YL-6100, YoungLin) was used quantitatively to analyze the concentration and the composition of the produced gas during the replacement reaction.

Gas hydrate formation process

Artificial glass beads (average particle size: 100 μm, detailed physical properties are shown in Supporting Information Table S1) were used to simulate a real NGH environment. After packing the glass beads 2–4 times on a vibrator, we injected ultrapure water into the high-pressure vessel. The initial porosity of the specimen was determined to be approximately 32%. In the early stage of this procedure, the degree of water saturation in the specimen was calculated using the difference between the volume of the ultrapure water used during the preparation of the specimen and the weight of the drained water, producing an irreducible water saturation rate of approximately at 45.9% after gas injection. 14.6% (e.g., $0.32 \times 0.459 \times 100\% = 14.6\%$) of the pore space is filled with the irreducible water phase, some of which will be transformed into methane hydrate. Subsequently, a pressure leak test was conducted at a constant pressure (10.05 MPa) and temperature (293.15 K). Once it was confirmed that there was no pressure leakage in the system, the temperature of the system was lowered to 274.15 K to form the CH_4 hydrate. The hydrate saturation (S_{hyd}) rate was calculated using the following equation proposed by Sakamoto et al.[39]

$$S_{hyd} = \frac{Q_{wt}}{172} \cdot \frac{\Delta P}{P_0} \cdot \frac{T_0}{T_f} \cdot \frac{1}{AL\Phi}$$

Here, the volume of methane gas stored per 1 m^3 of hydrate is assumed to be 172 m^3; Q_{wt} [m^3] is the volume of water displaced by the gas injection; ΔP [MPa] is the pressure drop due to the hydrate formation; P_0 [MPa] is pressure in the standard condition; T_0 [K] is the temperature in the standard condition; T_f [m^3] is the temperature used during the hydrate formation process; A [m^2] is the cross-sectional area of the geological porous media; L [m] is the length of the geological porous media, and Φ is the porosity of the porous media. After the initial hydrate formation process, an annealing process[40] was used to enhance the overall hydrate formation yield. The annealing process involves raising the temperature to 288.15 K and reforming the hydrate in the specimen by lowering the temperature to 274.15 K. Although the conversion rate of water to hydrate (ratio of formed methane hydrate to the irreducible water phase, not S_{hyd}) measured through the first formation stage was about 40%, the conversion rate increased to approximately 82% after the annealing process. With the successful application of the annealing process, most of the irreducible water phase was transformed into the methane hydrate phase. With less of the water phase, it is possible to observe the CH_4—CO_2 replacement reaction exclusively. After hydrate formation and pressure stabilization in the reactor, the CH_4 gas was refilled to the desired system pressure of 9.8 MPa. To ensure the reliability of the experimental setup, we performed a replacement reaction under two different hydrate saturations: (1) a high hydrate saturation (S_{hyd}) case, where an annealing process was adopted to enhance the hydrate conversion rate and (2) a low hydrate saturation (S_{hyd}) case, in which an annealing process was not adopted and where only the initial methane hydrate formation process was performed. Initially, we observed exothermic peaks from every sampling port in different positions during CH_4 hydrate formation. When the reactor temperature is lowered to gas hydrate forming conditions, gas hydrates start to form simultaneously throughout the reactor and exothermic peaks from each different port appear within 60 min time window. However, exothermic peaks are only an indication for gas hydrate formation within specimen and quantitative analysis on gas hydrate morphology is required. Therefore, the morphology and texture of the initial methane hydrate are predicted by pore-habit-specific models depending on the gas hydrate saturation proposed by Dai et al.[41] (Supporting Information Figure S1). In both hydrate saturation cases (high/low), the methane hydrate distribution is predicted as a homogeneous pore-filling (H_1) structure. Dai et al.[41] classified heterogeneous hydrate distribution types into (1) hydrate nodules and chunks in fine-grained sediments, (2) lenses and vein, and (3) patchy saturation. In contrast, pore-filling morphology is regarded as homogeneous gas hydrate distribution in the hydrate-bearing sediment.

Continuous replacement reaction

The gaseous mixture (CO_2 20 mol % and N_2 80 mol %) was injected at a constant flow rate after the hydrate formation was completed. Back pressure regulator effectively maintained the system pressure during the experiment. During the replacement process, the real-time GC analysis was performed at five ports, 0.7, 2.4, 4.0, 5.6, and 7.3 m. At each fluid sampling port customized line filter, PT-type thermocouple, pressure transducer, and sampling tube (0.006″ inner diameter) connected to the GC multiposition valve was installed. The multiposition valve was used to control sequential gas injection into the GC. In the low hydrate saturation experiment (no annealing process), clogging in the sampling line was occasionally observed because of the unreacted free water which remained in the reactor. However, the clogging problems were solved when we ran the same experiment at a high hydrate saturation rate with the full annealing process. The operating pressure and temperature conditions in this study were 9.8 MPa and 275.15 K, respectively. The actual replacement efficiency was calculated by deducting the produced methane gas volume from the GC compositional analysis. The replacement efficiency from each experiment was calculated using the following equation

$$\text{Replacement Efficiency}(\%) = \frac{\text{Volume of produced } CH_4 \text{ gas}}{\text{Volume of total injected } CH_4 \text{ gas}} \times 100(\%)$$

The volume of produced CH_4 gas was calculated from the totally produced gas volume, the totally injected CH_4 volume, and the compositional analysis from the GC results. The volume of CH_4 in the hydrate is the amount of gas consumed in the hydrate formation process which is proportional to the CH_4 volume injected in the refill.

Results and Discussion

We performed a blank test run before performing the complete replacement experiment to analyze gas compositional

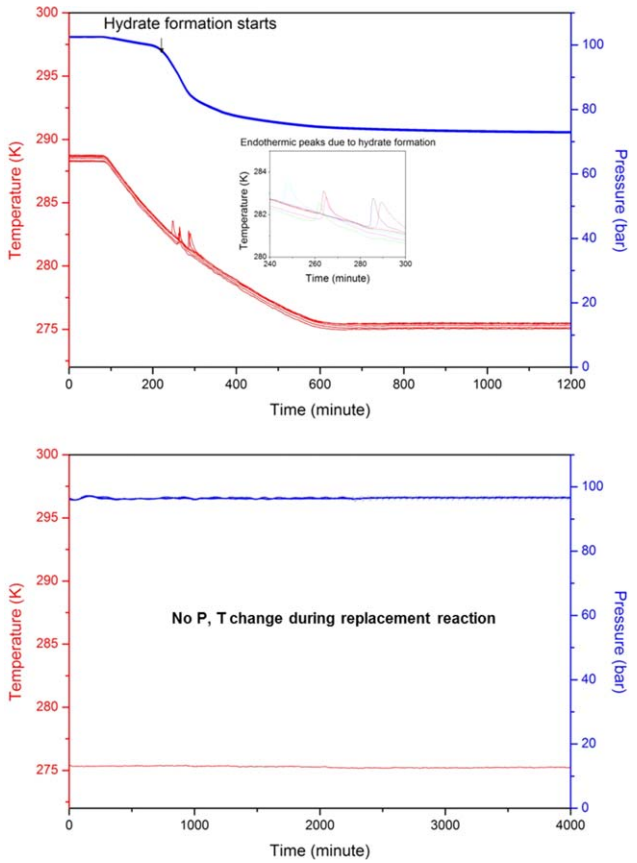

Figure 2. Temperature and pressure log data during hydrate formation-replacement process.

[Color figure can be viewed in the online issue, which is available at wileyonlinelibrary.com.]

changes (migration of CH_4 throughout the pressure vessel) without hydrates in the system ($S_{hyd} = 0\%$). The CH_4 displaced by the injected $CO_2 + N_2$ gas in the blank run was analyzed by GC and is shown in Supporting Information Figure S2 at a $CO_2 + N_2$ injection rate of 100 sccm. The methane concentrations at five ports started to decrease at a certain time, which is called "breakthrough." Time intervals between two adjacent ports were about 100–150 min. According to the blank run results (100 sccm), $CO_2 + N_2$ gas injection should be maintained for at least 1200 min to recover most of the gaseous methane gas from the specimen. After the initial blank test run, methane gas was recharged to start the formation of gas hydrates. When the system pressure and temperature were stabilized, $CO_2 + N_2$ gas was injected at rates of 50, 100, and 200 sccm, respectively. The pressure and temperature log during the whole process of "gas hydrate formation"-"$CO_2 + N_2$ gas injection" is shown in Figure 2. We also performed the same replacement experiments at two different hydrate saturation rates (high S_{hyd} and low S_{hyd}, as shown in Table 1). We mainly discuss the result of the high S_{hyd} case in the Results and Discussion section. The low S_{hyd} system contains a considerable amount of free water, which can affect the replacement rate and the smooth flow of the injected fluid. This can cause the formation of a pure $CO_2 + N_2$ mixed gas hydrate. We briefly discuss the result of the low S_{hyd} case in the last part of this section.

The gas composition profiles (CH_4, N_2, and CO_2) in the reactor as a function of the length are shown in Figure 3 at a $CO_2 + N_2$ injection rate of 50 sccm (high S_{hyd}). Initially, the pressure vessel was filled with four phases: glass beads (~68 vol %), methane hydrate (~12 vol %), a small volume of residual water (~3 vol %, water leftover after the methane hydrate formation), and methane gas (~17 vol %). Figure 3 shows the expected tendency that the CH_4 concentration decreases with time while the concentrations of CO_2 and N_2 increase with time. As the $CO_2 + N_2$ is injected, methane gas is displaced by $CO_2 + N_2$, triggering spontaneous replacement reaction in the hydrate phase. This integrated compositional information along the length becomes essential for establishing the flow-front of gases in the sandy gas hydrate layer and a reliable estimation of methane recovery. At the first and last sampling ports located 0.7 and 7.3 m away from the inlet, CH_4 breakthroughs appear around 150 and 900 min, respectively, just after $CO_2 + N_2$ injection. The total run time was counted when the methane level at the outlet is lower than 5% and for the 50 sccm run the total run time was 3200 min.

Here, we note that both CO_2 and N_2 sufficiently possess the guest exchange ability by attacking and replacing the encaged CH_4 in NGH-bearing sediments. A close examination of the population ratio of N_2/CO_2 along the 1-D flow path can provide further precise information revealing on-spot replacement efficiency and unique kinetic patterns during chemical exchange. At the initial replacement stage, the CO_2 molecules are vigorously consumed by their dominant occupancy in large cages while N_2 molecules participate in a more preferentially occupying small cage. Unlike CO_2 injection system, N_2/CO_2 in gas phase can be a convenient variable to see how the injected gases are consumed by CH_4 hydrate. Shin et al.[9] and Koh et al.[10] measured the CH_4 cage occupancy change during CH_4—(CO_2 or $CO_2 + N_2$) exchange reaction. In the case of CO_2 injection, CH_4 cage occupancy (small cage/large cage, initially 0.333) increased. It reflects that CO_2 mostly replace CH_4 in large cages. However, when CO_2/N_2 is injected, CH_4 cage occupancy ratio remained at initial value (0.333) throughout the replacement reaction. Addition of N_2 further replaces CH_4 in the small cages and thus CH_4 cage occupancy during exchange is remained same. From these experimental observations, we tried to use N_2/CO_2 ratio in gas phase to overlook the CH_4—($CO_2 + N_2$) exchange behavior. Accordingly, such a guest-specific preference to cage dimensions can lead to significant enhancement of methane recovery and a qualitative understanding of the replacement behavior. Initially injected mixed gas (80 mol % N_2 and 20 mol % CO_2) has N_2/CO_2 ratio of around four. As structure I gas hydrate has two small cages and six large cages in a unit cell [2(S) 6(L) $46H_2O$] and previous experiment observation allows us to assume constant decay ratio of CH_4 in large cage and small cage. In other words, ideally, CO_2 is consumed three times faster than N_2. Faster CO_2 consumption during replacement reaction results in increase in N_2/CO_2 ratio in gas phase. As shown in Figure 4a, the N_2/CO_2 ratio increased with time and distance from the inlet, reached the maximum (~500 min at the 0.7 m port, ~700 min at 2.4 m, ~900 min at 4.0 m, 1100 min at 5.6 m, and 1300 min at 7.3 m) and thereafter slowly decreased. Furthermore, according to the distance from the inlet, the peak values of the N_2/CO_2 ratio varied in the range of 5–10, which reveals more rapid consumption of CO_2 than N_2 during the replacement reaction. Assuming that outer gas hydrate layer started to be replaced by $CO_2 + N_2$ (ideal replacement efficiency ~85% reported

Table 1. Details of the Experimental Results for the Replacement Process

System	Injection Rate (sccm)	Initial Porosity (%)	Absolute Permeability (μm^2)	Irreducible Water Saturation	Hydrate Conversion (%)	Hydrate Saturation (S_{hyd}, %)	Run Time (min)	Replacement Efficiency at 7.3 m (%)
High S_{hyd}	50	32.1	0.217	45.1	82.50	11.94	3200	49.2
	100				81.03	11.73	1800	42.2
	200				81.27	11.76	1200	31.4
Low S_{hyd}	50	31.9	0.212	44.6	39.02	5.64	3200	23.1
	100				40.05	5.79	1800	20.5
	200				39.86	5.77	1200	15.9

by Park et al.), gas phase composition would be changed due to gas consumption during replacement reaction. As stated above, CO_2 is consumed faster than N_2, thus, N_2/CO_2 ratio in gas phase will increased from initial value of approximately 4. Once the mixed gas hydrate layer formed on the outer layer of gas hydrates, mixed gas hydrate layer inhibits the penetration of further diffusion of $CO_2 + N_2$ into CH_4 hydrate layer. Lee et al.[32] experimentally verified the diffusion limitation of liquid CO_2 injection into CH_4 hydrate. The authors showed the penetration depth is controlled by diffusion/reaction models. Similarly, our system has certain penetration limits and thus exhibits maxima in N_2/CO_2 ratio in gas phase. Figure 4b shows the total cumulative amount of gas at each port that increased with the distance from the inlet. For quantitative analysis, we calculated the replacement efficiency (i.e., the total CH_4 recovery) based on these GC results (Table 1). The 49% of CH_4 from gas hydrate was recovered using $CO_2 + N_2$ for a period of 3200 min. The replacement process results in Table 1 do not completely reflect the whole nature of real NGH sediments but can be effectively used for production-scale design.

Next, we increased the $CO_2 + N_2$ gas injection rate to 100 sccm. Figure 5 shows the gas compositional changes during 1800 min of run time. The first sampling port 0.7 m away from the inlet shows CH_4 breakthrough after 150 min of gas injection. The front of $CO_2 + N_2$ gas started to show up in the 7.3 m outlet after 600 min of injection. The overall CH_4 breakthrough time decreased as the $CO_2 + N_2$ injection rate increased to 100 sccm. The total run time was counted to 1800 min, which was shorter than that of the 50 sccm run.

The N_2/CO_2 ratio and the amount of cumulative gas for the 100 sccm run are shown in Figure 6. All of the N_2/CO_2 maximum peaks are located in the period of 600–800 min. The ratio values vary from 4 to 6 depending on the distance from the inlet and are relatively smaller than the results of the 50 sccm run. Figure 6b shows the amount of total

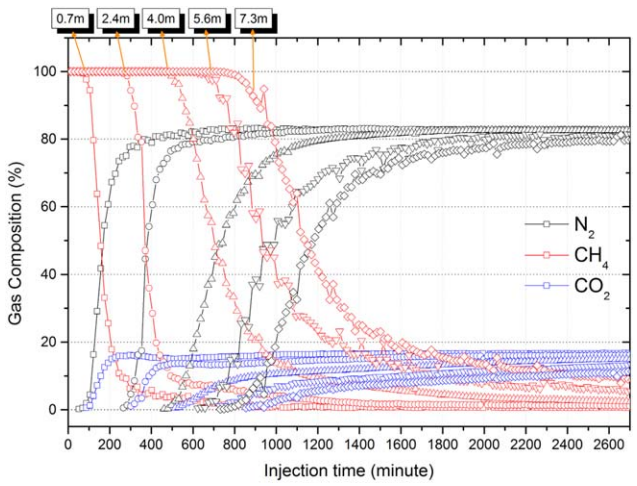

Figure 3. Integrated gas compositional profiles according to the distance from the inlet by real-time GC measurement at a $CO_2 + N_2$ gas injection rate of 50 sccm.

Red lines represent the fraction of CH_4, blue lines represent the fraction of CO_2, and black lines represent the fraction of N_2. Different symbols were used to distinguish the ports: Circles (○) correspond to port at 0.7 m, squares (□) to 2.4 m, triangles (Δ) to 4.0 m, inverted triangles (▽) to 5.6, and diamonds (¤) to 7.4 m. [Color figure can be viewed in the online issue, which is available at wileyonlinelibrary.com.]

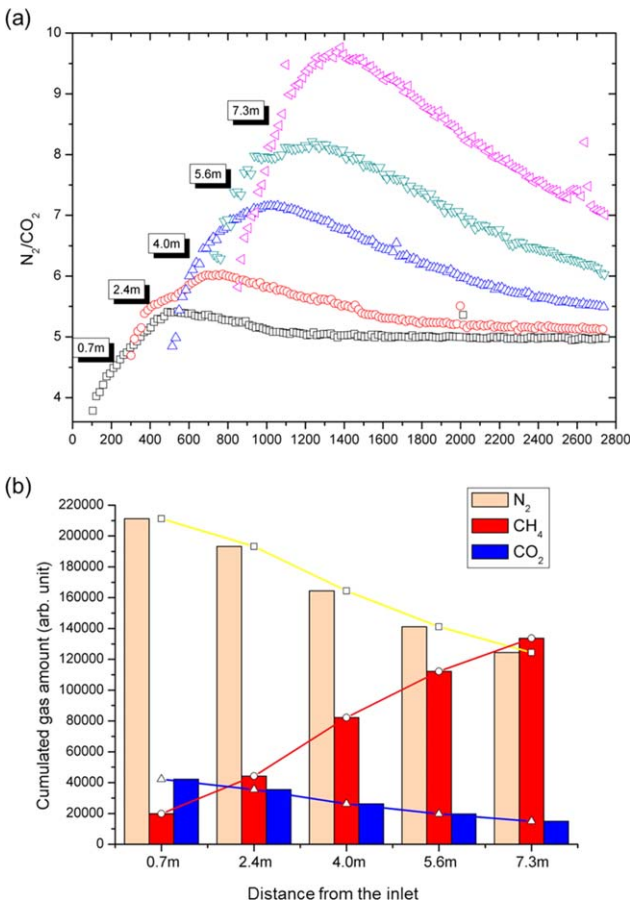

Figure 4. $CO_2 + N_2$ gas injection rate of 50 sccm: (a) The N_2/CO_2 ratio changes at each sampling port; (b) the cumulative produced gas amount at each port after 3200 min of $CO_2 + N_2$ gas injection.

[Color figure can be viewed in the online issue, which is available at wileyonlinelibrary.com.]

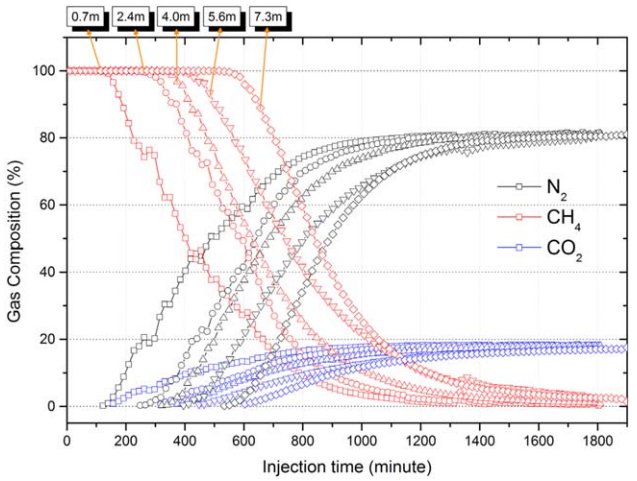

Figure 5. Integrated gas compositional profiles according to the distance from the inlet by real-time GC measurement at a $CO_2 + N_2$ gas injection rate of 100 sccm.

Red lines represent the fraction of CH_4, blue lines represent the fraction of CO_2, and black lines represent the fraction of N_2. Different symbols were used to distinguish the ports: Circles (○) correspond to port at 0.7 m, squares (□) to 2.4 m, triangles (Δ) to 4.0 m, inverted triangles (▽) to 5.6, and diamonds (⌑) to 7.4 m. [Color figure can be viewed in the online issue, which is available at wileyonlinelibrary.com.]

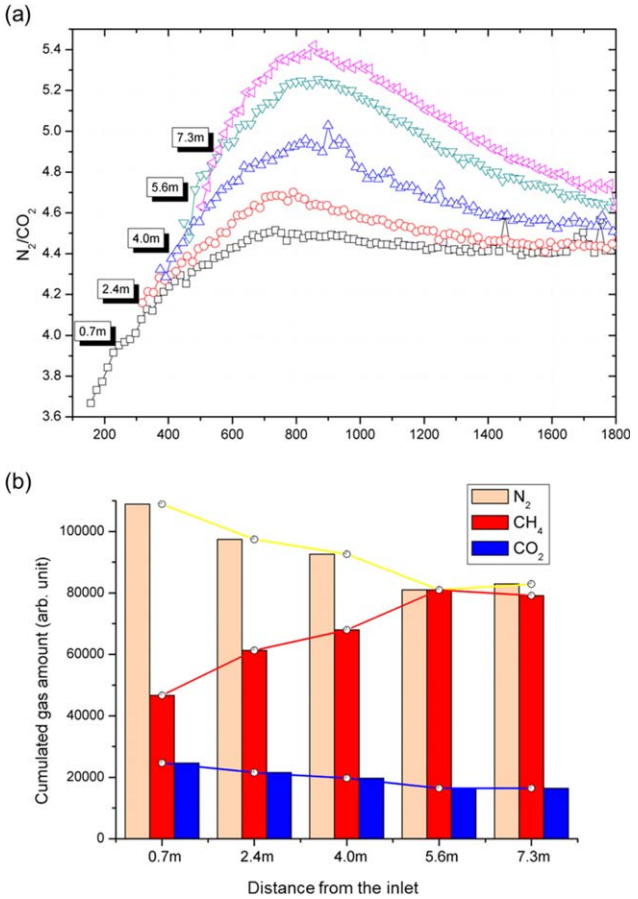

Figure 6. $CO_2 + N_2$ gas injection rate of 100 sccm: (a) The N_2/CO_2 ratio changes at each sampling port; (b) the cumulative produced gas amount at each port after 1800 min of $CO_2 + N_2$ gas injection.

[Color figure can be viewed in the online issue, which is available at wileyonlinelibrary.com.]

cumulative gas produced at each port after 1800 min, which smoothly increased with the distance until it reached 5.6 m from the inlet. The CH_4 recovery rate stopped increasing after 5.6 m and became congested. In the real field test, the desired gas hydrate production range (length) and estimated recoverable gas amount (volume) should be precisely decided for a successful test. Quantitative analysis of evolved gases showed that the replacement efficiency of the 100 sccm run decreased about 14% compared to the results of the 50 sccm run. The total runtime decreased about 35% as the injection rate increased to 100 sccm.

Again, we doubled-up the $CO_2 + N_2$ injection rate to 200 sccm (Figure 7). During 1200 min of run time, the gas compositions changed sharply inside the pressure vessel, demonstrating a CH_4 breakthrough time of 300 min at 7.3 m from the inlet and an overall CH_4 breakthrough time of 50–300 min. The run time also decreased in the 200 sccm injection run as the CH_4 was rapidly depleted in the reactor. When the $CO_2 + N_2$ injection rate increased to 200 sccm, all of the maximum N_2/CO_2 peaks were located in 100–400 min (Figure 8a). The N_2/CO_2 varied from 4 to 7 depending on the distance from the inlet. However, we observe that the N_2/CO_2 did not constantly increase as in the results of the 50 and 100 sccm injection runs. Rather, the maximum peaks were focused on 2.4–4.0 m from the inlet. As the injection rate increased to 200 sccm, the replacement reaction occurred mainly at 2.4–4.0 m from the inlet, and the N_2/CO_2 ratio suddenly dropped at 5.6–7.3 m. Figure 8b shows the total amount of cumulative produced gas at each port after 1200 min. The cumulative amount of CH_4 abruptly increased after 2.4 m. The CH_4 recovery rate evolved in the 2.4–5.6 m section and afterward congested. For the quantitative analysis, the replacement efficiency of the 200 sccm run based on these GC results is shown in Table 1. When compared to the results of the 50 sccm run and the 100 sccm run, the replacement efficiency of the 200 sccm run decreased about 36% and 26%, respectively. In contrast, the total run time decreased about 35% and 23%, respectively. The $CO_2 + N_2$ gas injection rate was inversely proportional to the replacement efficiency, whereas the total run time was significantly shortened.

The changes in the $CO_2 + N_2$ gas injection rate significantly changed the behavior of the replacement reaction in the 1-D experiment. The two main variables, replacement efficiency and total run time, were sensitively changed according to the $CO_2 + N_2$ gas injection rate. As shown in Figure 9a, a high flux of $CO_2 + N_2$ gas resulted in shallow penetration to the gas hydrate layers due to short residence time, and thus replacement efficiency decreased. Otherwise, the low flux of the $CO_2 + N_2$ gas results allowed deep penetration to the gas hydrate layers and demonstrated higher replacement efficiency. In addition, we present the low S_{hyd} case results in Table 1. With a low hydrate saturation in the reactor, approximately 8.5 vol % of the reactor is filled with the unreacted free-water phase (only 3% of the unreacted water phase remained in the high hydrate saturation case). The untransformed water (free-water) phase may sufficiently react with the injected $CO_2 + N_2$ gas mixture to a form pure $CO_2 + N_2$ hydrate and eventually hinder a complete understanding of the actions which occur inside the 8 m reactor.

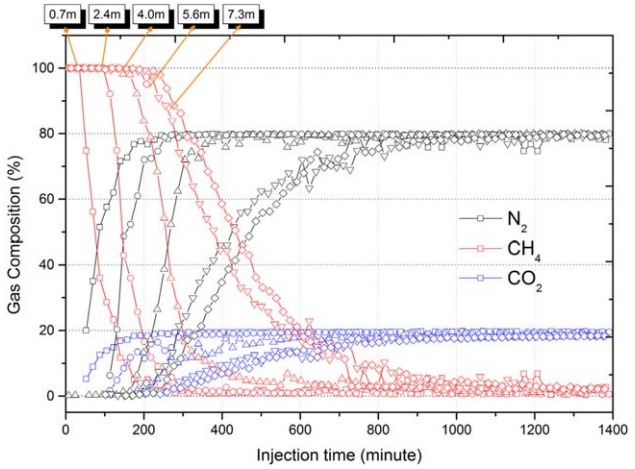

Figure 7. Integrated gas compositional profiles according to the distance from the inlet by real-time GC measurement at a $CO_2 + N_2$ gas injection rate of 200 sccm.

Red lines represent the fraction of CH_4, blue lines represent the fraction of CO_2, and black lines represent the fraction of N_2. Different symbols were used to distinguish the ports: Circles (○) correspond to port at 0.7 m, squares (□) to 2.4 m, triangles (Δ) to 4.0 m, inverted triangles (▽) to 5.6, and diamonds (⌑) to 7.4 m. [Color figure can be viewed in the online issue, which is available at wileyonlinelibrary.com.]

Moreover, clogging occurs occasionally during a continuous $CO_2 + N_2$ injection into the reactor. These results suggest that one should be aware of the effect of free water in the reservoir when designing gas production tests which involve a CH_4—CO_2 replacement reaction. As shown in Table 1, the low hydrate saturation results show significantly low replacement efficiency rates (15–23%). To focus on the replacement reaction, we tried to eliminate the free-water phase by applying an annealing process which would greatly enhance the hydrate saturation rate. We assume, in the high hydrate saturation case, that most of the mobile free-water phase is transformed into the methane hydrate phase and that the remaining 3 vol % of the free-water phase is out of the gas diffusion limit range in the space. Therefore, we concentrated on the results of the high hydrate saturation case in an effort to observe the replacement reaction more accurately.

The qualitative comparison of the N_2/CO_2 ratio vs. the injection rate is shown in Figure 9b. The N_2/CO_2 ratio visualizes the behavior of replacement front during whole run time. Thick solid lines represent the connection line between the maximum points in each graph. In the 50 sccm run, the replacement reaction occurred in a gentle manner throughout the whole run time as the injection rate was relatively slow. When the injection rate was doubled up to 100 sccm, the slope of the red solid line steeply increased compared to the black solid line of the 50 sccm run. A further increase in the injection rate to 200 sccm abruptly changed the replacement behavior in the reactor. A sharp peak appeared in the early part of the injection and the reaction diminished after 600 min of injection. These qualitative changes in the N_2/CO_2 ratio are due to the fluid contact time and mass transfer capacity into the methane hydrate layer. At the lowest possible injection rate in the 50 sccm run, a fully widespread replacement reaction occurs throughout the reactor, shown as a successive increment in the maximum peaks in each port. However, the total run time nearly doubles when compared to the 100 and 200 sccm run times. In the medium case of the 100 sccm run, a successive increment in the maximum peaks is also observed, but the absolute values are lower than those in the 50 sccm run. We also conjecture that a replacement reaction occurs throughout the reactor with a shorter run time than in the 50 sccm in 100 sccm runs. However, at the highest volumetric injection rate of 200 sccm, distinct sharp peaks arise in the first and second fluid sampling ports, and the peak diminishes after the third fluid sampling port. It is assumed, at this high volumetric injection rate, that a vigorous replacement reaction occurs around the inlet and that the replacement front may not be uniformly distributed past a certain distance away from the inlet. The vigorous replacement reaction which occurred in the early ports may result in a sudden increase in the partial pressure of CH_4 in the fluid mixture; thus, the replacement capacity decreases past a certain point. This trend is also represented as the lowest total CH_4 recovery yield among the three injection rates (Table 1).

For the quantitative analysis of replacement efficiency, the compositions of produced gas along 1-D length are shown in Figure 10. Replacement efficiencies of each run in Table 1 are based on the CH_4 proportions from Figure 10 and the total produced gas volume. Table 1 and Figure 10 show the quantitative analysis of the replacement efficiencies

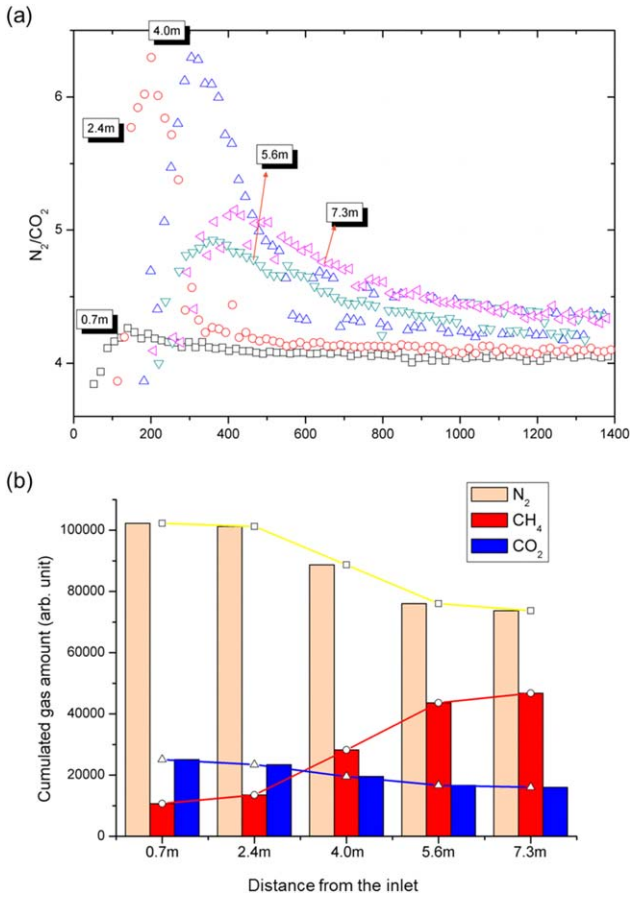

Figure 8. $CO_2 + N_2$ gas injection rate of 200 sccm: (a) N_2/CO_2 ratio changes at each sampling port. (b) Cumulative produced gas amount at each port after 1200 min of $CO_2 + N_2$ gas injection.

[Color figure can be viewed in the online issue, which is available at wileyonlinelibrary.com.]

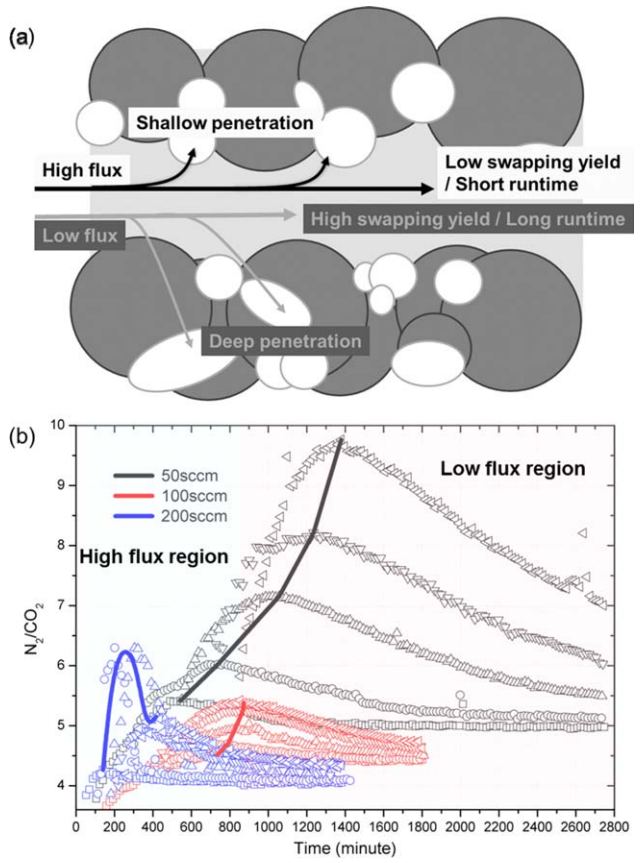

Figure 9. (a) Schematic illustration of the high/low flux situation; (b) N_2/CO_2 ratio changes at each sampling port with a varying $CO_2 + N_2$ gas injection rate: 50, 100, and 200 sccm.

[Color figure can be viewed in the online issue, which is available at wileyonlinelibrary.com.]

depending on the distance from the inlet and the gas injection rate. A maximum of 49% of the replacement efficiency resulted from the 50 sccm run and the replacement efficiency

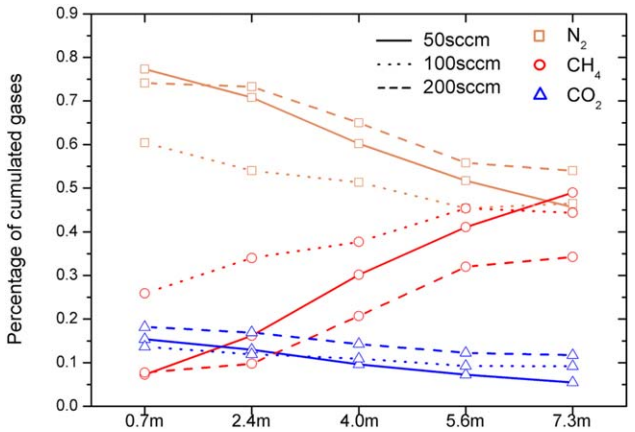

Figure 10. Percentage of total cumulated gases from each port at three different injection rates.

Solid lines represent the results from the 50 sccm run, dotted lines represent the results from the 100 sccm run, and dashed lines represent the results from the 200 sccm run. Symbols indicate gas molecules; orange squares represent N_2, red circles represent CH_4, and blue triangles represent CO_2. [Color figure can be viewed in the online issue, which is available at wileyonlinelibrary.com.]

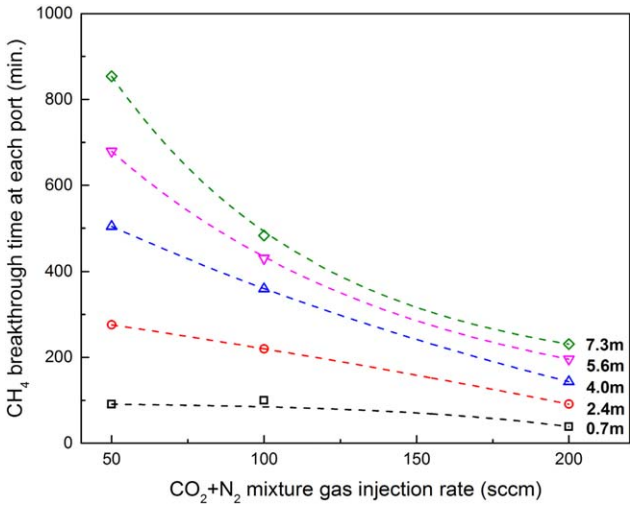

Figure 11. CH_4 breakthrough time for each sampling ports (0.7–7.3 m) depending on the CO_2/N_2 injection rates.

[Color figure can be viewed in the online issue, which is available at wileyonlinelibrary.com.]

decreased as the injection rate increased. However, in the real production scheme, the time constraint is critical and it is essential to optimize productivity in a limited time window. As expected from Figure 10, CH_4 productivity is closely connected with the gaseous flow in 1-D scale. For a real production scheme, from these results, the optimum distance between injection and production wells could be deduced. Furthermore, the run times for both injection and methane gas recovery rates can be roughly inferred from this graph, which would be used as a tool for making decision in the operation of a production well and establishing the overall methane hydrate production plans. Also, CH_4 breakthrough time for each ports depending on the CO_2 + N_2 injection rates are shown in Figure 11. CH_4 breakthrough times for Port 1–3 (0.7–4.0 m) were linearly regressed, however, exponentially regressed to fitting the CH_4 breakthrough times for Ports 4 and 5 (5.6–7.3 m). In other words, CH_4 breakthrough time exponentially increases at low CO_2 + N_2 injection rate when the reaction length is longer than 5.6 m.

Furthermore, experimental variables obtained from the experiments were compared with physical models of diffusion/reaction to examine the kinetic trends in replacement reaction in 1-D scale. Methane replacement efficiencies depending on CO_2/N_2 gas injection rates are fitted with Avrami crystallization kinetics model[42,43] (Figure 11 and Table 2) using following equation

$$\alpha = 1 - \exp\left(-k_1 t^n\right)$$

where, α is the hydrate conversion ratio at time t, k is the rate constant with the growth stage, and n is the Avrami exponent. Replacement reaction has similar physical changes of crystallization, therefore, it first occurs at the hydrate surface and further diffusion of CO_2/N_2 into the inner layers allow the propagation of replacement reaction. As shown in Figure 12, Avrami model is well-fitted with both high S_{hyd} case and low S_{hyd} case. This is largely due to the nature of continuous-flow scheme of $CO_2 + N_2$ gas mixture during the whole experiments because Avrami model is applicable in the initial reaction stage in the hydrate films. In every experiments, $CO_2 + N_2$ mixture gas injection was stopped

Table 2. Parameters Regressed for Avrami Model

System	k_1	n
High S_{hyd}	0.07534	0.55909
Low S_{hyd}	0.05706	0.39116

when the methane level at the outlet is lower than 5%. Unlike soaking experiments, which use static CO_2 pressure, our experimental scheme uses dynamic $CO_2 + N_2$ pressure. Therefore, penetration into the methane hydrate is shallow and overall kinetics follows the Avrami model. Low Avrami exponent values (Table 2) suggest that mass transfer in the continuous-flow system is limited by diffusion controlled replacement reaction. In summary, our experimental continuous-flow replacement reaction in 1-D scale is dominated by fast surface replacement reaction.

For the successful employment of the replacement reaction in a real production plan, one must consider many other factors influencing the actual productivity on-site. To test the concept of CH_4 replacement with $CO_2 + N_2$, a complete understanding of the $CO_2 + N_2$ replacement mechanism under complex sediment structure is necessary. For the testing of CH_4—$(CO_2 + N_2)$ replacement in bench-scale, we built a new reactor with 1-D functionality (8 m) and conducted continuous gas injection experiments. Also we tried to simulate the hydrate-bearing sediment at specified conditions of pressure and temperature by forming pore-filling type gas hydrates within glass beads. The qualitative movement of complex multiphase fluids was analyzed and further quantitative productivity assessments were performed with three gas injection rates of 50, 100, and 200 sccm. Several key variables of $CO_2 + N_2$ gas injection rate, total run time, CH_4 breakthrough, and CH_4 recovery rate were also clearly examined.

The key findings are as follows: (1) replacement efficiency is inversely proportional to the $CO_2 + N_2$ gas injection rate as the decrease in the injection rate corresponds to an increase in the productivity due to an increase in contact time. Adequate contact time is needed for replacement reaction to proceed smoothly. However, in the production field, if a production test is performed with a very low $CO_2 + N_2$ gas injection rate or with an extended run time, problems can arise related to production delay and increased operation cost. Thus, an ideal critical injection rate and the amount of injected $CO_2 + N_2$ gas should be determined during the establishment of a quantitative production plan; (2) propagation of the frontline of multicomponent fluid was analyzed in a scale of 8 m. Qualitative analysis on the compositional profiles at each port indicated that at least 5.6 m is needed to show an understandable recovery rate in this system. Extension of this variable will assist the design of an injection/production well; and (3) ideal replacement efficiency obtained (~85%) from a microscopic approach on the hydrate in the bulk state was revealed to be lower (~49%). Complex flow of a multicomponent fluid and the lowered diffusivity in the porous media are the main reasons for restraints for lowered replacement efficiency.

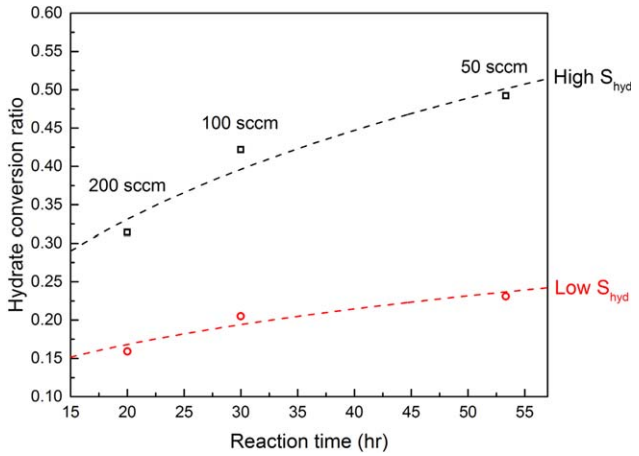

Figure 12. Avrami model fitting (dashed lines) for CH_4 replacement efficiencies according to $CO_2 + N_2$ injection rates.

[Color figure can be viewed in the online issue, which is available at wileyonlinelibrary.com.]

Acknowledgments

This research was funded by the Ministry of Knowledge Economy through the "Recovery/Production of Natural Gas Hydrate using Swapping Technique" project [KIGAM—Gas Hydrate R&D Organization]. It was also supported by a grant from the National Research Foundation Korea (NRF) funded by the Korean government (MEST) (No. 2010-0029176) and by the WCU program (31-2008-000-10055-0), funded by the Ministry of Education and Science and Technology.

Literature Cited

1. Boswell R, Collet TS. Current perspectives on gas hydrate resources. *Energy Environ Sci.* 2011;4:1206–1215.
2. U.S. DOE, Methane hydrate newsletter. *Fire in the ice*. 2011;11:1–5.
3. Japan Oil, Gas and Metals National Corporation, Gas Production from Methane Hydrate Layers Confirmed, JOGMEC, 2013. Available at: www.jogmec.go.jp/english/news/release/release0110.html. Last accessed on November 19, 2014.
4. U.S. E.I.A (Energy Information Administration), Technically Recoverable Shale Oil and Shale Gas Resources: an Assessment of 137 Shale Formations in 41 Countries Outside the United States, Analysis and Projections, 2013, http://www.eia.gov/analysis/studies/worldshalegas/, Last accessed on November 19, 2014.
5. Bahk JJ, Kim GY, Chun JH, Kim JH, Lee JY, Ryu BJ, Lee JH, Son BK, Collet TS. Characterization of gas hydrate reservoirs by integration of core and log data in the Ulleung Basin, East Sea. *Mar Pet Geol.* 2013;47:30–42.
6. Ohgaki K, Takano K, Sangawa H, Matsubara T, Nakano S. Methane exploitation by carbon-dioxide from gas hydrates-phase-equilibria for CO_2–CH_4 mixed hydrate system. *J Chem Eng Jpn.* 1996;29:478–483.
7. Lee H, Seo Y, Seo YT, Moudrakovski IL, Ripmeester JA. Recovering methane from solid methane hydrate with carbon dioxide. *Angew Chem Int Ed.* 2003;42:5048–5051.
8. Park Y, Kim DY, Lee JW, Huh DG, Park KP, Lee J, Lee H, Sequestering carbon dioxide into complex structures of naturally occurring gas hydrates. *Proc Natl Acad Soc USA.* 2006;103:12690–12694.
9. Shin K, Park Y, Cha M, Park KP, Huh DG, Lee H, Kim SJ, Lee H. Swapping phenomena occurring in deep-sea gas hydrates. *Energy Fuels.* 2008;22:3160–3163.
10. Koh DY, Kang H, Kim DO, Park J, Cha M, Lee H. Recovery of methane from gas hydrates intercalated within natural sediments using CO_2 and a CO_2/N_2 gas mixture. *ChemSusChem.* 2012;5:1443–1448.
11. Uchida T, Ikeda IY, Takeya S, Kamata Y, Ohmura R, Nagao J, Zatsepina OY, Buffett BA. Kinetics and stability of CH_4–CO_2 mixed gas hydrates during formation and long-term storage. *ChemPhysChem.* 2005;6:646–654.
12. Li ZZ, Guo XQ, Wang JB, Yang LY. Experiment studies on CH_4 recovery from hydrate using CO_2 in different systems. *Nat Gas Ind.* 2008;28:129–132.
13. Zhao J, Xu K, Song Y, Liu W, Lam W, Liu Y, Xue K, Zhu Y, Yu X, Li Q. A review on research on replacement of CH_4 in natural gas hydrates by use of CO_2. *Energies.* 2012;5:399–419.
14. Li ZZ, Guo XQ, Chen GJ, Wang JB, Yang LY, Wang T. Experimental and kinetic studies on methane replacement from methane hydrate formed in SDS system by using pressurized CO_2. *J Chem Ind Eng China.* 2007;58:1197–1203.

15. Geng CY, Wen H, Zhou H. Molecular simulation of the potential of methane reoccupation during the replacement of methane hydrate by CO_2. *J Phys Chem A*. 2009;113:5463–5469.
16. Fan Y, Liu DP, Xie YM, Zhong DL, Xiao Y. Feasibility analysis on replacement of CH_4 from hydrate sediment by CO_2. *Nat Gas Geosci*. 2007;18:317–320.
17. Ota M, Morohashi K, Abe Y, Watanabe M, Smith RL, Inomata H. Replacement of CH_4 in the hydrate by use of liquid CO_2. *Energy Convers Manage*. 2005;46:1680–1691.
18. Zhou XT, Fan SS, Liang DQ, Du JW. Determination of appropriate condition on replacing methane from hydrate with carbon dioxide. *Energy Convers Manage*. 2008;49:2124–2129.
19. Zhang W, Wang Z, Li WQ, Li WY, He DW. Research progress in the enhanced replacing methane out of gas hydrate by carbon dioxide emulsion. *Nat Gas Chem Eng*. 2009;34:9–63.
20. Jayasinghe AG, Grozic JLH. An experimental investigation of temperature induced dissociation of methane hydrate in porous media. In: *Proceedings of the 6th International Conference on Gas Hydrates (ICGH)*. Vancouver, Canada, 2008.
21. Lee JY, Santamarina JC, Ruppel C. Parametric study of the physical properties of hydrate-bearing sand, silt, and clay sediments: 1. Electromagnetic properties. *J Geophys Res: Solid Earth*. 2010;115:B11.
22. Lee S, Lee Y, Lee J, Lee H, Seo Y. Experimental verification of methane–carbon dioxide replacement in natural gas hydrates using a differential scanning calorimeter. *Environ Sci Technol*. 2013;22:13184–13190.
23. Tan CP, Freij-Ayoub R, Clennell MB, Tohidi B, Managing wellbore instability risk in gas hydrate-bearing sediments. In: *SPE Asia Pacific Oil & Gas Conference and Exhibition (SPE)*. Jakarta, Indonesia, 2005.
24. Bai D, Zhang X, Chen G, Wang W. Replacement mechanism of methane hydrate with carbon dioxide from microsecond molecular dynamics simulations. *Energy Environ Sci*. 2012;5:7033–7041.
25. Zhou X, Fan S, Liang D, Du J. Replacement of methane from quartz sand-bearing hydrate with carbon dioxide-in-water emulsion. *Energy Fuels*. 2008;22:1759–1764.
26. Zhou Y, Castaldi MJ, Yegulalp TM. Experimental investigation of methane gas production from methane hydrate. *Ind Eng Chem Res*. 2009;48:3142–3149.
27. Yuan Q, Sun CY, Yang X, Ma PC, Ma ZW, Liu B, Ma QL, Yang LY, Chen GJ. Recovery of methane from hydrate reservoir with gaseous carbon dioxide using a three-dimensional middle-size reactor. *Energy*. 2012;40:47–58.
28. Yuan Q, Sun CY, Liu B, Wang X, Ma ZW, Ma QL, Yang LY, Chen GJ, Li QP, Li S, Zhang K. Methane recovery from natural gas hydrate in porous sediment using pressurized liquid CO_2. *Energy Convers Manage*. 2013;67:257–264.
29. Ota M, Saito T, Aida T, Watanabe M, Sato Y, Smith RL, Inomata H. Macro and microscopic CH_4–CO_2 replacement in CH_4 hydrate under pressurized CO_2. *AIChE J*. 2007;53:2715–2721.
30. Ota M, Abe Y, Watanabe M, Smith J, Richard L, Inomata H. Methane recovery from methane hydrate using pressurized CO_2. *Fluid Phase Equilib*. 2005;228–229:553–559.
31. Hirohama S, Shimoyama Y, Wakabayashi A, Tatsuta S, Nishida N. Conversion of CH_4-Hydrate to CO_2-Hydrate in liquid CO_2. *J Chem Eng Jpn*. 1996;29:1014–1020.
32. Lee BR, Koh CA, Sum AK. Quantitative measurement and mechanisms for CH_4 production from hydrates with the injection of liquid CO_2. *Phys Chem Chem Phys*. 2014;16:14922.
33. Yeon SH, Seol J, Koh DY, Seo YJ, Park KP, Huh DG, Lee J, Lee H. Abnormal methane occupancy of natural gas hydrates in deep sea floor sediments. *Energy Environ Sci*. 2011;4:421–424.
34. Yeon SH, Seol J, Seo YJ, Park Y, Koh DY, Park KP, Huh DG, Lee J, Lee H. Effect of interlayer ions on methane hydrate formation in clay sediments. *J Phys Chem B*. 2009;113:1245–1248.
35. Jakobsen M, Hudson JA, Minshull TA, Singh SC. Elastic properties of hydrate-bearing sediments using effective medium theory. *J Geophys Res*. 2000;105(B1):561–577.
36. Helgerud MB. Wave speeds in gas hydrate and sediments containing gas hydrate: a laboratory and modeling study. Ph.D. dissertation, Stanford University, Stanford, California, 2001.
37. Sakai A. Can we estimate the amount of gas hydrates by seismic methods? Gas Hydrates: Challenges for the Future. *Ann NY Acad Sci*. 2000;912:374–391.
38. Kvalstad TJ, Yamamoto K, Noguchi S, Uchida S, Soga K. Effect of gas hydrate production on seabed stability in the eastern nankai trough area. In: *Proceedings of the 7th International Conference on Gas Hydrates (ICGH)*. Edinburgh, Scotland, United Kingdom, 2011.
39. Sakamoto Y, Komai T, Haneda H, Kawamura T, Tenma N, Yamaguchi T. Experimental study on modification of permeability in a methane hydrate reservoir and gas production behavior by the simultaneous injection of nitrogen and hot water. In: *Proceedings of 5th International Conference on Gas Hydrates (ICGH)*. Trondheim, Norway, 2005:866–874.
40. Hyodo M, Nakata Y, Yoshimoto N, Ebinuma T. Basic research on the mechanical behavior of methane hydrate sediments mixture, *Soils Found*. 2005;45:75–85.
41. Dai S, Santamarina JC, Waite WF, Kneafsey TJ. Hydrate morphology: physical properties of sands with patchy hydrate saturation. *J Geophys Res: Solid Earth*. 2012;117:B11.
42. Avrami M. Kinetics of phase change. I. General theory. *J Chem Phys*. 1939;7:1103.
43. Avrami M. Granulation, phase change, and microstructure kinetics of phase change. III. *J Chem Phys*. 1941;9:177.

Manuscript received June 1, 2014, and revision received Oct. 17, 2014.